DISLOCATIONS STRUCTURE AND SCATTERING PHENOMENON IN CRYSTALLINE CELL SIZE OF 2024 AL ALLOY DEFORMED BY ONE PASS OF ECAP AT ROOM TEMPERATURE

M. H. Goodarzy[1] *, H. Arabi[2], M. A. Boutorabi[2], S. H. Seyedein[1] and H. Shahrokhi[3]

* *mh_goodarzy@iust.ac.ir*

Received: July 2013 **Accepted: November 2013**

[1] School of Metallurgy and Materials Engineering, Iran university of Science & Technology, Tehran, Iran.

[2] Center of Excellence for High Strength Alloys Technology (CEHSAT), School of Metallurgy and Materials Engineering, Iran University of Science and Technology, Tehran, Iran.

[3] Department of mechanical Engineering, Azad University Saveh Branch, Iran.

Abstract: *Variation in microstructural features of 2024 aluminum alloy plastically deformed by equal channel angular pressing (ECAP) at room temperature, was investigated by X-Ray diffraction in this work. These include dislocation density; dislocation characteristic and the cell size of crystalline domains. Dislocations contrast factor was calculated using elastic constants of the alloy such as C_{11}, C_{22} and C_{44}. The effect of dislocations contrast factor on the anisotropic strain broadening of diffraction profiles was considered for measuring the microstructural features on the base of the modified Williamson-Hall and Warren-Averbach methods. Results showed that the dislocations density of the solution annealed sample increased from $4.28\times10^{12}m^{-2}$ to $2.41\times10^{14}m^{-2}$ after one pass of cold ECAP and the fraction of edge dislocations in the solution annealed sample increased from 43% to 74% after deformation. This means that deformation changed the overall dislocations characteristic more to edge dislocations. Also the crystalline cell size of the solution annealed sample decreased from 0.83μm to about 210nm after one pass of ECAP process at room temperature.*

Keywords: *ECAP, 2024 aluminum alloy, XRD, peak broadening, dislocation contrast factor*

1. INTRODUCTION

Age hardenable aluminum alloys, 2xxx and 7xxx series are considerably used in aerospace industry. Severe plastic deformation of these alloys has been utilized in the two last decades to improve their mechanical properties [1, 2]. Increase in dislocation density of sever plastically deformation of materials and their interaction with the gowning dislocation are known as the main mechanism of strengthening in these alloys [3, 4]. In recent years it has been revealed that X-ray diffraction instrument is a powerful means for determining the microstructural parameters such as dislocations characteristics. Using dislocation contrast factor in data processing of XRD results has some abilities for investigating dislocation densities, type of the prevailing dislocations and the cell size distribution [5-7].

According to Ungar [8] in the presence of strain anisotropy the deviation from the ideal diffraction pattern can be conceived as: (I) peak shift, (II) peak broadening, III) peak asymmetries and (v) peak shape. Modified Williamson-Hall and Warren-Averbach techniques using contrast factor of dislocations are adequate for modeling the diffraction peak profiles in the presence of strain anisotropy [6 & 9]. Usually severe plastic deformation processes generate strain anisotropy in deformed material. Geng et al. [10] have reported that diffraction peaks of Al-3.3Mg alloy are shifted after ECAP process. Referring to work of Ungar et al. [5] who evaluated peak broadening of ECAPed Copper, the use of classical Williamson-Hall plot revealed a strong strain anisotropy in deformed copper, consequently modified Williamson-Hall technique for peak profile analysis was used in this work.

In this research, the X-ray peak profile analysis of a 2024 Al alloy after severe plastic deformation by one pass of ECAP at room temperature which has not been reported elsewhere according to the best knowledge of the

authors for this alloy, have been evaluated using modified Williamson-IIall and Warren-Averbach techniques.

2. EXPERIMENTAL PROCEDURE

2. 1. Materials

Commercial aluminum alloy 2024-T8 in the form of extruded rod with mean chemical composition of Al–4.2Cu-1.26Mg-0.63Mn-0.42Fe–0.29Si (in wt. %), was deformed by equal-channel angular pressing (ECAP) after solution annealing treatment. Cylindrical specimens with a diameter of 11.7 mm and length of 70 mm were solution annealed at 500 °C for 40 minutes and quenched in water prior to ECAP processing. Severe plastic deformation by ECAP was conducted at room temperature for one pass on the quenched sample using a die with an inner angle of 90° and an outer angle of 22.5°. For this die design, according to Iwahashi equation [11] the effective strain resulted per pass through the die was1.05

2. 2. XRD Measurements

X-ray diffraction analysis was carried out on the polished sections of the solution annealed and deformed samples in a SEIFERT-3003TT diffractometer using Cu K_α radiation of 0.15406 nm wavelength, 40 kV and 50 mA with a scan rate of 0.005o/s. In order to minimize the effect of initial texture effect on the diffraction peaks, XRD data were obtained from the longitudinal and transvers sections of the initial rod and then averaged to construct intensities for a complete diffraction diagram. Experimental XRD peak data of a coarse grained pure aluminum with negligible structural broadening was used to remove instrumental broadening from the experimental X-ray diffraction peak data of the studied samples according to stoke method[12].

2. 3. XRD Peak Analysis

In the classic Williamson–Hall method, the full width at half maximum (FWHM) of separate diffraction peaks are drawn versus diffraction vector $K=2\sin(\theta)/\lambda$, where θ and λ are Bragg's angle of the peak and the X-ray wavelength of Cu (K_α) radiation, respectively. The ordinate intersection and the slope of the linear plot confirming to the measured data, determine the average crystalline cell size and values of the lattice micro strain, respectively [13]. Generally, the strain anisotropy causes an infirmity in using of the classical Williamson–Hall method for peak broadening of data obtained from XRD measurements. In order to modeling of the peak broadening in the presence of the strain anisotropy, average dislocation contrast factor, $\bar{c}$ was calculated for studied material according to the Ungar procedure [5]. In this work average crystalline cell size, density of dislocations and characteristic of prevailing dislocations were determined by XRD peak profile analysis according to the modified Williamson–Hall and Warren–Averbach methods using dislocation contrast factor [5, 9, 14, and 15]. A brief explanation of these methods is as follow:

2. 3. 1. The modified Williamson–Hall Method

Full widths at half maximum (FWHM) of experimental diffraction peaks of the studied alloys are determined as the widths of pseudo-voigt function fitted to the experimental diffraction data which is the combination of Gaussian and Cauchy functions. The structural peak widths are determined according to the Stokes method as given $\Delta K=\Delta K_{exp}-\Delta K_i$, where ΔK, is related to the structural FWHM and ΔK_{exp}, and ΔK_i are the experimental and instrumental FWHMs, respectively. After reduction of the instrumental broadening from the measured FWHM, the structural FWHM or the integral breadth (β) diffraction peaks are drawn vs. $KC^{\frac{1}{2}}$ as given by Ungar et al [16]:

$$\Delta K = FWHM = \frac{0.9}{d} + \left(\frac{\pi R^2 b^2}{2}\right)^{\frac{1}{2}} \rho^{\frac{1}{2}} \left(K\bar{C}^{\frac{1}{2}}\right) + O(K^2\bar{C}) \qquad (1)$$

$$\beta = \frac{1}{D} + \left(\frac{\pi \hat{R}^2 b^2}{2}\right)^{\frac{1}{2}} \rho^{\frac{1}{2}} \left(K\bar{C}^{\frac{1}{2}}\right) + O(K^2\bar{C}) \qquad (2)$$

When d and D are the apparent sizes of the cell corresponding to the FWIIM and the integral breadth which are determined by extrapolating $KC^{\frac{1}{2}}$ to zero. R and R´ are constants depending on the effective outer cut-off radius of dislocations, K=2sin(θ)/λ, O indicates non-interpreted higher-order terms, b is the length of the Burgers vector of dislocations, ρ is the dislocation density, and $\bar{C}$ is the average contrast factor of dislocations. It is demonstrated that in polycrystalline cubic metals include random orientation and random population of Burgers vectors in active slip systems, the value of $\bar{C}$ is calculated by the following equation [5]:

$$\bar{C}_{hkl} = \bar{C}_{hoo}(1 - qH^2) \quad (3)$$

When $\bar{C}_{hoo}$ is the average dislocation contrast factor of (h00) plane, q is the character of the dislocation parameter related to the crystal elastic constants and fraction of screw or edge type of dislocations. H^2 is the hkl index of the different reflections that for a specific reflection (hkl) can be determined by:

$$H^2 = \frac{(h^2k^2 + h^2kl^2 + k^2l^2)}{(h^2 + k^2 + l^2)^2} \quad (4)$$

Theoretical values of $\bar{C}_{hoo}$ and also characteristic parameter of dislocation, q_{th} are calculated numerically for pure edge (q_{th}^{edge}) and pure screw dislocations (q_{th}^{screw}) in different slip systems according to the elastic constants of the crystal structure. By squaring of equation (1) and neglecting the higher order terms, it can be represented by [5, 16]:

$$FWHM^2 = \left(\frac{0.9}{d}\right)^2 + \left(\frac{\pi R^2 b^2}{2}\right)\rho(K^2\bar{C}) \quad (5)$$

Inserting equation (3) into (5) yields [5]:

$$\frac{FWHM^2 - \alpha}{K^2} = \omega\bar{C}_{hoo}(1 - qH^2) \quad (6)$$

When, $\alpha = \left(\frac{0.9}{d}\right)^2$ and $\omega = \frac{\pi R^2 b^2 \rho}{2}$. From the linear regression of the left-hand side of equation (6) versus H^2, the experimental characteristic parameter of dislocation, q_{exp} can be determined and the fraction of prevailing edge and screw dislocations will be calculated by using of (q_{th}^{edge}) and (q_{th}^{screw}) according to lever rule as given by [17] :

$$f^{screw} = 1 - f^{edge} = \frac{q_{th}^{edge} - q_{exp}}{q_{th}^{screw} - q_{th}^{edge}} \quad (7)$$

2. 3. 2. The modified Warren–Averbach method

In the Warren–Averbach method [18], the profile of each diffraction peak is converted into corresponding Fourier form which can be given as the multiplication of the size (A^S_L) and distortion coefficients (A^D_L).

$$A_L = A^S_L * A^D_L \quad (8)$$

Warren [17] has shown that the Fourier coefficient of each diffraction profile, A_L, can be written as:

$$\ln A_L \cong \ln A_L^S - 2\pi^2 L^2 K^2 \langle \varepsilon_k^2 \rangle \quad (9)$$

When L is the Fourier length, K is the diffraction vector and $\langle \varepsilon_k^2 \rangle$ is the mean square strain caused by dislocations in the direction of the diffraction vector [19]. For small values of L it can be written as:

$$\langle \varepsilon_k^2 \rangle \cong (\rho\bar{C}b^2/4\pi)\ln(R_e/L) \quad (10)$$

When ρ is the density of dislocations, Re is the effective outer cut-off radius and $\bar{C}$ is the average dislocation contrast factor. By inserting equation (10) into equation (9) and transforming to the form of a power series, the modified

Warren–Averbach equation is obtained as [5, 13, and 20];

$$\ln A_L \cong \ln A_L^S - \rho\frac{\pi b^2}{2}L^2 \ln\left(\frac{R_e}{L}\right)(K^2\bar{C}) + O(K^2\bar{C}) \qquad (11)$$

When O is small and stands for higher orders of $K^2\bar{C}$. For various values of L, Fourier size coefficient, A_L^S is determined by extrapolating of equation (11) at $K^2\bar{C}$=0. In the diagram of A_L^S versus L, intercept of the slope of linear part of the diagram at A_L^S=0, gives the area-weighted column length denoted by Lo and can be equal to average cell size of dislocations [9].

In order to determine the density of dislocations, second term of equation (11) must be separately evaluated by defining H (L) as:

$$H(L) = \rho\frac{\pi b^2}{2}L^2 \ln\left(\frac{R_e}{L}\right) \qquad (12)$$

Afterwards dividing equation (12) by L^2, a linear equation between H (L)/L^2 versus Ln (L) is obtained as:

$$\frac{H(L)}{L^2} = \rho\frac{\pi b^2}{2}[\ln(R_e) - \ln(L)] \qquad (13)$$

Plotting H (L)/L^2 versus Ln(L) gives density of dislocations (ρ) and effective outer cut-off radius of dislocations (R_c) by a linear regression. Subsequently, the mean spacing between dislocations, $L=\rho^{-0.5}$, is determined.

3. RESULTS

XRD diagrams of solution annealed and deformed samples are illustrated in Fig. 1. The XRD data for the solution annealed sample were obtained from the longitudinal and transvers

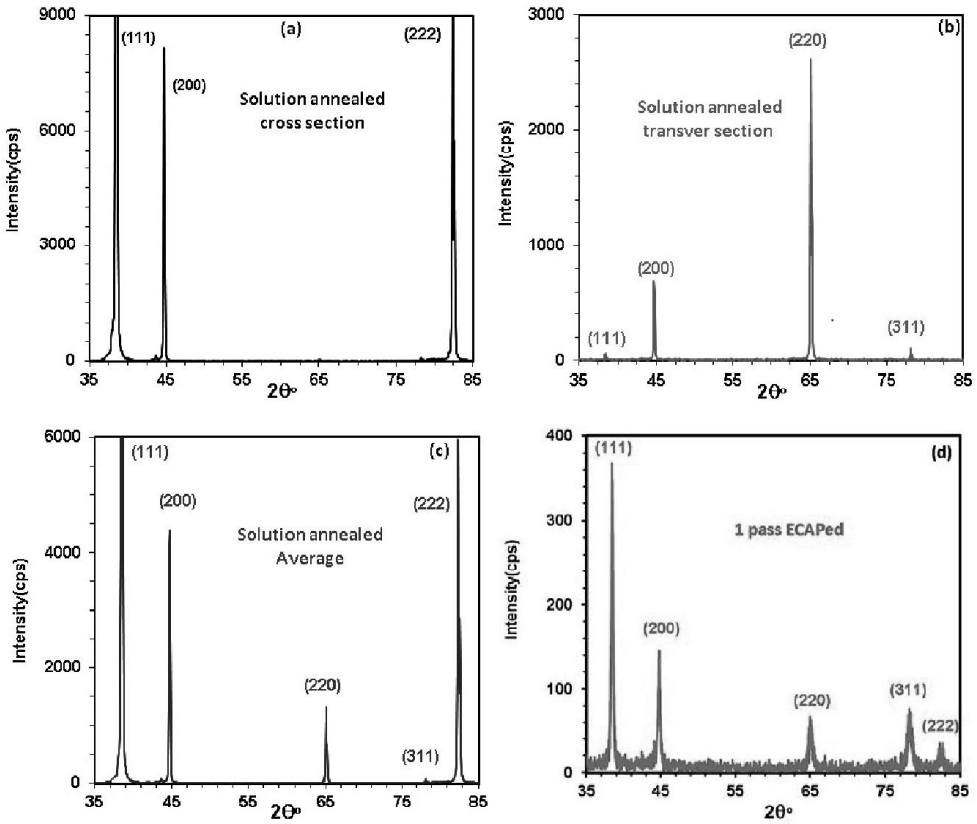

Fig. 1. XRD pattern of (a) the solution annealed sample obtained from cross section (b) the solution annealed sample obtained from the longitudinal section; (c) the solution annealed sample per average data obtained from the longitudinal and cross sections; (d) the deformed sample by one pass of ECAP obtained from cross section.

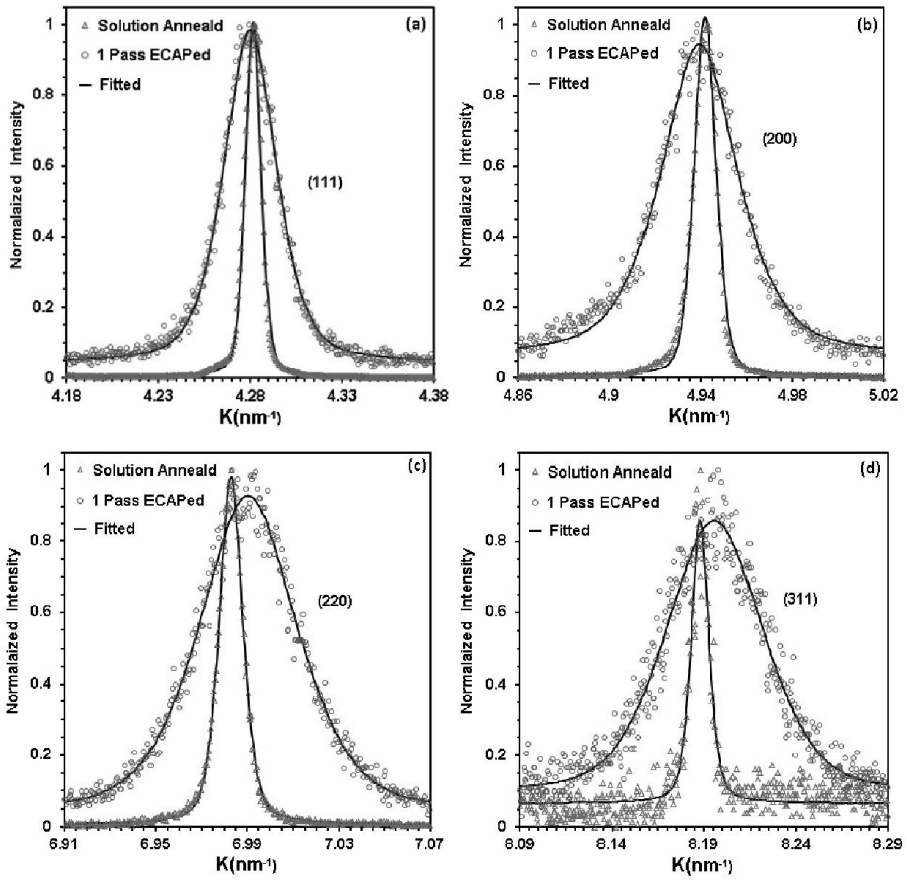

Fig. 2. Measured and fitted XRD peaks after normalizing vs. diffraction vector on the solution annealed and the deformed sample (a) (111) diffraction; (b) (200) diffraction; (3) (220) diffraction; (d) (311) diffraction

sections as shown in Fig. 1(a & b). In order to minimize the initial texture effect on the XRD analysis, the average of these data shown in Fig. 1(c) was considered for data processing. The diffraction peaks are broadened and their intensities are sharply decreased after one pass of ECAP at room temperature as shown in Fig. 1(d). According to references of [8, 21] this is due to an increases in lattice defects include linear and planar defects.

In order to analyze the peak broadening phenomenon, Rachinger's correction method [22] was used for separating $k\alpha_1$and $k\alpha_2$ peaks in each diffraction peak of solution annealed sample. Then the average intensities in each peak profile were plotted against diffraction vector $K=2Sin\theta/\lambda$; where θ and λ are the Bragg's angle of the peak, and the wave length of Cu ($K\alpha$), respectively. The Experimental data points of intensities versus the diffraction vector $K=2Sin\theta/\lambda$ were normalized to unity and fitted along with a pseudo-voigt function, as shown in Fig. 2.

The scattering of diffraction data and peak broadening of the deformed sample is more than those of the solution annealed sample especially in higher order diffraction as shown in Fig. 2. According to Ungar [8] this can be due to an increase in linear defects specially dislocations formed during severe plastic deformation. Also the peaks shift which is shown in Fig. 2, expresses the considerable amount of distortion in the lattice structure of the deformed materials, since according to Ungar [8] the peaks shift can be related to long range stresses as well as sub grain boundaries generated by deformation. The FWHM values of

Table 1. The FWHM and Integral breadth (β) of solution annealed and ECAPed samples of 2024 Al Alloy.

Diffraction line	Solution Annealed		1Pass ECAPed	
	FWHM(nm^{-1})	β(nm^{-1})	FWHM(nm^{-1})	β(nm^{-1})
(111)	0.00421	0.00511	0.0301	0.04026
(200)	0.00520	0.00605	0.03721	0.04968
(220)	0.00605	0.00718	0.04520	0.05551
(311)	0.00645	0.00761	0.04852	0.05753
(222)	0.00715	0.00811	0.05653	0.06731

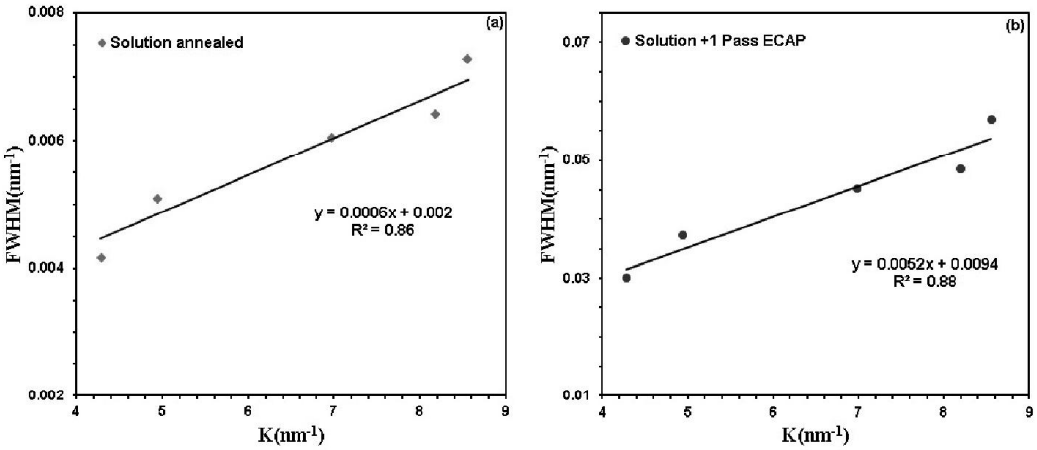

Fig. 3. Classic Williamson–Hall diagram of the alloys; (a) Solution annealed and (b) the ECAPed samples

the reflections after removal of instrumental broadening are summarized in Table 1.

The Classic Williamson–Hall diagram, which is FWHM versus K, of the material is shown in Fig. 3. Due to relative strain anisotropy, the plots of the samples in Fig.3 show that the diffraction points correspond fairly to a straight line.

Assuming elastic constants for this material; C_{11} = 81.1GPa, C_{12} = 54.4GPa, and C_{44} = 26.7GPa [23], edge and screw dislocations of {111} <110> slip system, the average contrast factor of dislocations, $\bar{C}_{th}^{edge}$ and $\bar{C}_{th}^{screw}$,were calculated using the elastic anisotropy coefficients of $A_i = 2C_{44}/(C_{11} - C_{12}) = 0.5$ and $(C_{12}/C_{44}) = 2.04$ and on the relative orientation of the line and Burgers vectors of dislocations and the diffraction vector, according to the procedure presented by Ungar et al [5]. The values of $\bar{C}_{th}^{edge}$, $\bar{C}_{th}^{screw}$ and $\bar{C}_{th}^{Avr}$ are listed in Table 2. The later constant was obtained assuming an equal fraction of screw and edge type dislocations. Subsequently, using equation (6) theoretical character parameters of dislocation, q_{th}^{screw} and q_{th}^{screw} were calculated as 1.1631 and 2.0205, respectively.

In order to determine experimental dislocation character, q_{exp} a linear regression of the left hand side of equation (6) versus H^2 was plotted using optimum values as shown in Fig. 4. Subsequently, intercept points of those lines with horizontal axis determined the value of q_{exp} for the solution annealed and the deformed samples equal 1.667

Table 2. The calculated values of dislocation contrast factors for the diffracted lines of the studied alloys.

Diffraction line	$\bar{C}_{screw}$	$\bar{C}_{Edge}$	$\bar{C}_{Avr}$
111	0.07855	0.154925	0.116738
200	0.235733	0.252867	0.2443
220	0.117867	0.179383	0.148625
311	0.1617	0.206742	0.184221
222	0.07855	0.154925	0.116738

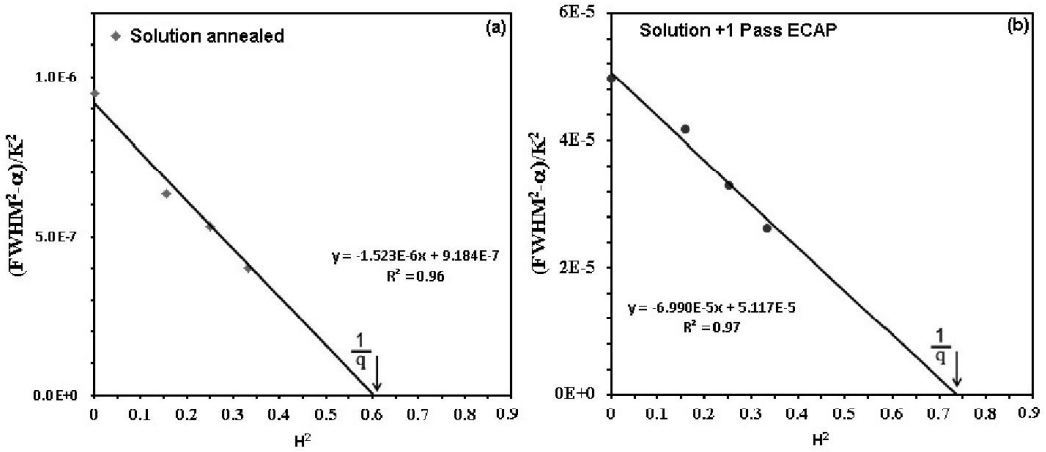

Fig. 4. Plot of $\frac{FWHM^2-\alpha}{K^2}$ versus H^2 for determining the experimental values of q_{exp} in (a) the solution annealed and (b) the deformed samples.

and 1.3698, respectively. By using equation (7), the ratio of edge dislocations to screw dislocations were determined 43:57 and 76:24 for the solution annealed and ECAPed samples, respectively.

Fig. 5. Shows modified Williamson–Hall diagrams for the solution annealed and the ECAPed samples. Extrapolation of the quadratic regressions of the FWHMs at $KC^{0.5}=0$ give apparent cell size parameter d, about 0.840 μm and 225 nm for solution annealed and the ECAPed samples, respectively.

Modified Warren–Averbach plots for the alloy are shown in Fig. 6. These plots were obtained by plotting $Ln(A_L)$ vs. K_2C at various amounts of Fourier length L according to equation (11). Extrapolating the plots at $K_2C=0$ give size Fourier coefficient (A_L^S) which is plotted vs. L in Fig. 7. The Middle data pointes on the plots of A_L^S vs. L were fitted into a line; the intercept of which with horizontal axis gives an area-weighted column length of L_0 = 810 nm and 195nm for the solution annealed and the deformed sample, respectively. These values are in accordance with those obtained in modified Williamson–Hall method. Dislocation density (ρ) and spacing between the dislocations were obtained from the plot of $H(L)/L^2$ vs. ln L as shown in Fig. 8.

4. DISCUSSION

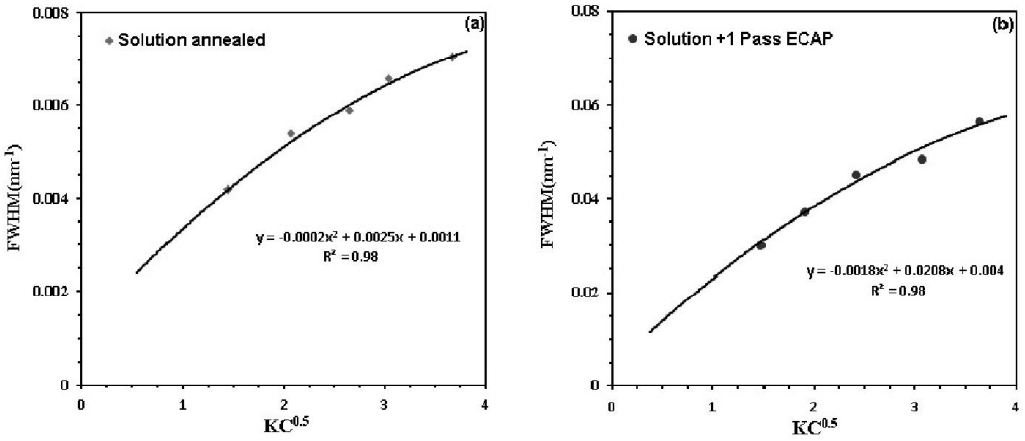

Fig. 5. Plots of FWHM versus $KC^{0.5}$ representing apparent size parameter in (a) the solution annealed and (b) the deformed samples.

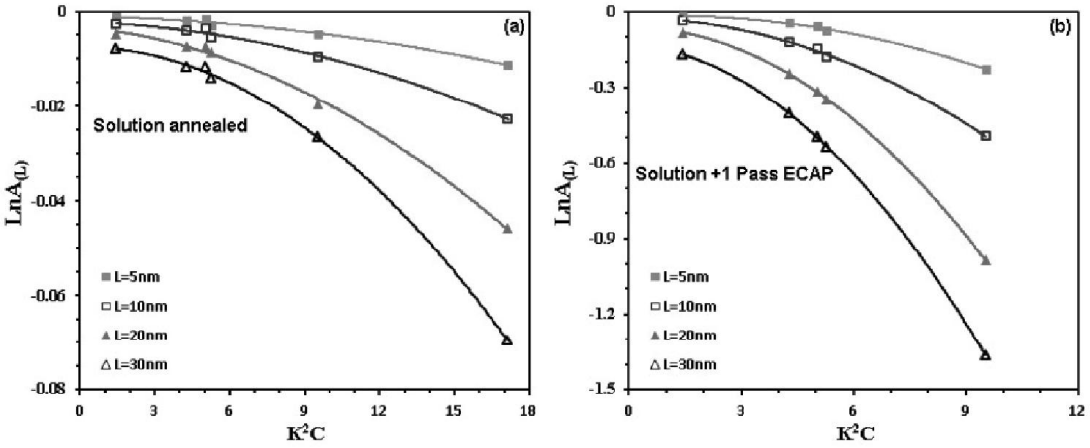

Fig. 6. Modified Warren-Averbach plots of (a) solution annealed and (b) the ECAPed samples.

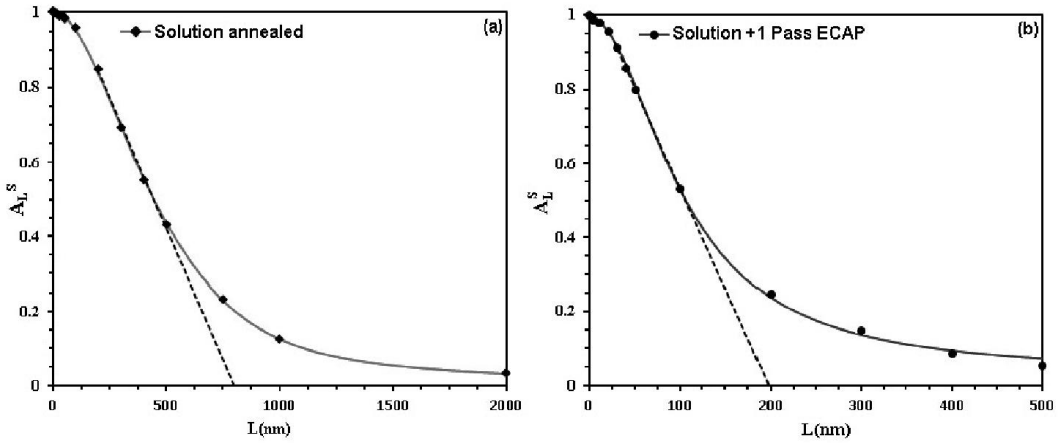

Fig.7. Plot of Size Fourier coefficient A_L^S versus L for (a) the solution annealed sample and (b) the deformed sample.

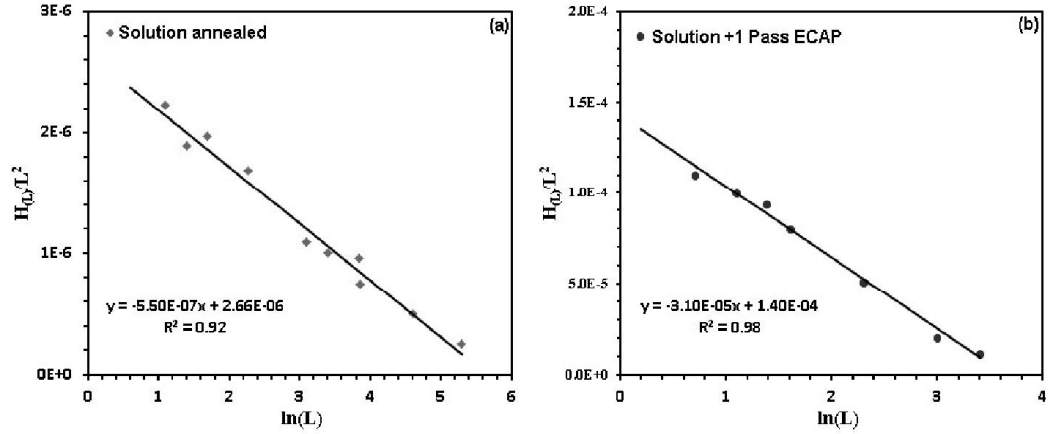

Fig. 8. Linear regression of H (L)/L^2 vs. Ln (L) determining the dislocation density and the dislocation spacing for (a) the solution annealed sample and (b) the deformed sample.

Microstructural parameters obtained from X-ray diffraction are listed in Table 3. Upon ECAP process of solution annealed 2024 Al alloy the following changes were detected; (i)dislocation density increased from $4.28\times10^{12}m^{-2}$ up to $2.41\times10^{14}m^{-2}$, (ii) the average of crystalline cell size decreased from about 0.83 m to about 210nm, (iii) the dislocation parameter q decreased from 1.56 to 1.37, That is to say that the fraction of edge dislocations increased from about 43% up to 74% and (iv) the mean spacing between dislocations decreased from 483 to 64 nm.

The obtained result is in accordance with results of other works [3, 4]. Zhao et al. [3] have reported that dislocation density of 7075 Al alloy, calculated by XRD data analysis after two passes of ECAP, increased to $9.4\times10^{14}m^{-2}$. Also according to Gubizca et al. [4], dislocation density of an Al-Zn-Mg-Cu alloy after two passes of ECAP increased to $3.4\times10^{14}m^{-2}$. The increase in dislocation density of 2024 Al alloy, measured in this study by a factor of about 70 times after one pass of ECAP, can sharply increase the yield stress of the deformed material. Also as shown in Table 3 due to increase in dislocation density after one pass of ECAP, the dislocation spacing L is obviously decreased. This can influence the amount of work hardening of the deformed sample which in turn can affect other mechanical properties of the alloy.

It has been well known that the apparent cell size determined by X-ray peak profile analysis is corresponding to the coherent crystalline cells size which is separated from each other by very small misorientation, up to few degrees [24]. According to the some reports in the deformed materials having submicron-size microstructure, dislocation cells separated by geometrically necessary dislocation boundaries having high angle of misorientation, whereas in the nanocrystalline materials, dislocation cells separated by incident dislocation boundaries with low angle of misorientation, [25-27]. In severe plastically deformed metals, dislocations cells considerably assist to incoherent scattering of X-

Table 3. Microstructural parameters of the studied materials by X-ray diffraction peak profile analysis.

Sample	d(nm)	L_o(nm)	$\rho(m^{-2})$	$L=\rho^{-0.5}$(nm)	q	%Edge dis.
Solution annealed (S)	845	810	4.28E+12	483	1.66	43
1 pass ECAPed (SE)	225	195	2.41E+14	64	1.37	74

ray diffraction. Therefore, the apparent cell size obtained for the studied alloy can correspond to the submicron-grain size. As shown in Table.3 the mean apparent grain size of the solution annealed sample decreased from 0.83 μm to about 210nm after one pass of ECAP. This result is in accordance with those reported by Ungar et al. [8]. They reported that submicron grain size of a copper rod having initial grain size about 300 μ decreases to 350nm after deformation by ECAP process.

The calculated values of the character of the prevailing dislocations, q for edge and screw dislocations in 2024 aluminum alloy are equal to 1.16 and 2.02, respectively. The random mixed character mean of q is equal to 1.59. An experimental value lower or higher than this value indicates the dominances of edge or screw type, respectively. Table 3 shows that in the materials used in this research, especially in the ECAPed sample the character of dislocations is edge type rather than screw type. This is in good conformity with model of severe plastic deformations which the screw dislocations are mainly annihilated during large deformations at room temperature [1, 28, and 29]. Rezvanifar et al [30] reported that for an Al-Si alloy, prevailing dislocation parameter q was shifted to pure screw dislocations during sever wear process but according to Gubicza et al [31] in the severe plastically bulk deformation of FCC metals the dislocation parameter q generally decreases with increasing strain. Consequently, one may conclude that the fraction of edge dislocations measured in 2024 Al alloy used in this study increased during ECAP process at room temperature.

4. CONCLUSIONS

2024 Al alloy was severe plastically deformed by one pass of ECAP process at room temperature after solution annealing. XRD peak profile analysis was used based on modified Williamson-Hall and Warren-Averbach techniques for verification of microstructural variations during severe plastic deformation. The main results obtained are as follow:

1. Strain anisotropy in the lattice of material was calculated successfully by the dislocation contrast factor.
2. Dislocation density of the material increased significantly due to severe plastically deformation at room temperature, however the amount of increase in fraction of edge segments was much more than screw segments during ECAP.
3. Cell size parameter in Al 2024 alloy decreased to one-fourth of its initial values after one pass of ECAP process at room temperature.

5. ACKNOWLEDGEMENTS

The corresponding author is grateful to Dr. M. R. Movaghar for his kind helps in data processing of XRD results.

REFERENCE

1. Valiev, R. Z., Islamgaliev, R. K. and Alexandrov, I. V., "Bulk nanostructured materials from severe plastic deformation", Prog. Mater. Sci. 45, 2000, 103-89.
2. Valiev, R. Z. and Langdon, T. G., "Principles of equal-channel angular pressing as a processing tool for grain refinement", Prog. Mater. Sci. 51, 2006, 881-981.
3. Zhao, Y., Liao X., Jin Z., Valiev R. and Zhu Y., "Microstructures and mechanical properties of ultrafine grained 7075 Al alloy processed by ECAP and their evolutions during annealing", Acta Mater. 52, 2004, 4589-99.
4. Gubicza, J., Schiller, I., Chinh, N., Illy, J., Horita, Z. and Langdon, T., "The effect of severe plastic deformation on precipitation in supersaturated Al–Zn–Mg alloys", Mater. Sci. Eng. A. 460, 2007, 77-85.
5. Ungar, T., Dragomir, I., Revesz, A. and Borbely, A., "The contrast factors of dislocations in cubic crystals: the dislocation model of strain anisotropy in practice", J. Appl. Cryst. 32, 1999, 992-1002.
6. Ungar, T., Gubicza, J., Ribarik, G., and Borbely, A., "Crystallite size distribution and dislocation structure determined by diffraction profile

analysis: principles and practical application to cubic and hexagonal crystals", J. Appl. Cryst. 34, 2001 298-310.
7. Ribarik, G., "Modeling of diffraction patterns based on microstructural properties", PhD Thesis, Eotvos Lorand University, 2008.
8. Ungar, T., "Microstructural parameters from X-ray diffraction peak broadening", Scrp. Mater. 51, 2004, 777-81.
9. Ribarik, G., Ungar, T. and Gubicza, J., "MWP-fit: a program for multiple wholeprofile fitting of diffraction peak profiles by ab initio theoretical functions", J. Appl. Crys. 34, 2001, 669-676.
10. Geng, H. B., Kang, S. B. and Min, B. K., "High temperature tensile behavior of ultra-fine grained Al–3.3Mg–0.2Sc–0.2Zr alloy by equal channel angular pressing", Mate. Sci. Eng. A 373, 2004, 229–238.
11. Iwahashi, Y., Horita, Z., Nemoto, M., Wang, J. and Langdon, T. G., "Principle of equal-channel angular pressing for the processing of ultra-fine grained materials", Scripta. Mater. 1996, 35, 143-146.
12. Warren, B. E., "X-ray Diffraction: Courier Dover Publications", 1969.
13. Williamson, G. and Hall, W. "X-ray line broadening from filed aluminium and wolfram", Acta Metall. 1953, 1, 22-31.
14. Culllity, B. D., "Elements of X-Ray Diffraction", Wiley, USA, 1976.
15. Wilkens, M., "The determination of density and distribution of dislocations in deformed single crystals from broadened X-ray diffraction profiles", Phys. Stat. Sol. A. 2, 1970, 359-370.
16. Ungar, T. and Borbely, A., "The effect of dislocation contrast on X-ray line broadening: a new approach to line profile analysis", App. Phys. Lett. 69, 1996, 3173- 3175.
17. Movaghar Garabagh, M. R., Hussein Nedjad, S., Shirazi, H., Iranpour Mobarekeh, M. and Nili Ahmadabadi, M., "X-ray diffraction peak profile analysis aiming at better understanding of the deformation process and deformed structure of martensitic steel", Thin Solid Films 516 2008, 8117–8124.
18. Warren, B. E., and Averbach, B. L., "The effect of cold work distortions on X-ray pattern", J. Appl. Phys. 21, 1950, 595-610.
19. Wilkens, M., "X-ray line broadening and mean square strains of straight dislocations in elastically anisotropic crystals of cubic symmetry", Phys. Stat. Sol. A 104 ,1987, K1-k6.
20. Zaefferer, S., "New developments of computer-aided crystallographic analysis in transmission electron microscopy", J. Appl. Cryst.. 33, 2000, 10-15.
21. Dragomir, I. C., Gheorghe, M., Thadhani, N. and Snyder, R. L., "X-ray peak profile analysis of crystallite size distribution and dislocation type and density evolution in nano-structured Cuobtained by deformation at liquid nitrogen temperature", Mater. Sci. Eng. A 402, 2005, 158–162.
22. Rachinger, W. A., "A Correction for the Kα1 Kα2 Doublet in the Measurement of Widths of X-ray Diffraction Lines", J. scien. Instru. 25, 1948,254-260.
23. Zhang, Y. K., "Elastic properties modification in aluminum alloy induced by laser-shock processing", Mater. Sci. Eng. A 297, 2001, 138–143.
24. Ungar, T., Ribarik, G., Gubicza, J. and Hanak, P., "Dislocation structure and crystallite size distribution in plastically deformed metals determined by diffraction profile analysis", J. of Eng. Mater. Tech. Trans. ASME, 124, 2002, 2–6.
25. Tolaminejad, B., Karimi Taheri, A., Arabi, H. and Shahmiri, M. , "An investigation into the effect of ECAE process on mechanical and microstructural properties of middle layer in copper clad aluminium composite", Iranian J. Mater. Sci. Eng., 2009, 6(4), 38-45.
26. Kuhlmann-Wilsdorf, D. and Hansen, N., "Geometrically necessary, incidental and subgrain boundaries", Scripta Metall. Mater. 25, 1991, 1557-1563.
27. Li, B. L., Godfrey, A., Meng, Q. C, Liu, Q. and Hansen, N., "Microstructural evolution of IF-steel during cold rolling", Acta Mater. 52, 2004, 1069-1075.
28. Estrin, Y., Molinari, L., Toth, S. and Brechet, Y., "A dislocation-based model for all hardening stages in large strain deformation", Acta Mater. 46, 1998, 5509-5515.
29. Ungar, T., Gubicza, J., Hanak, P., Alexandrov,

I., "Densities and character of dislocations and size-distribution of subgrains in deformed metals by X-ray diffraction profile analysis", Mater. Sci. Eng. A 319–321, 2001, 274–278.

30. Rezvanifar, A. and Zandrahimi, M., "Evaluation of dislocation structure and crystallite size in worn Al-Si alloy by X-ray diffraction" Iranian J. Mater. Sci. Eng., 2010, 7(1), 32-38.
31. Gubicza, J., Kassemc, M., Ribarik, G. and Ungar T., "The microstructure of mechanically alloyed Al–Mg determined by X-ray diffraction peak profile analysis", Mater. Sci. Eng. A 372, 2004, 115–122.